Supporting Information

A Study of Microwave Actuation of Liquid Crystalline Elastomer

S-Ⅰ: The preparation of LCE.

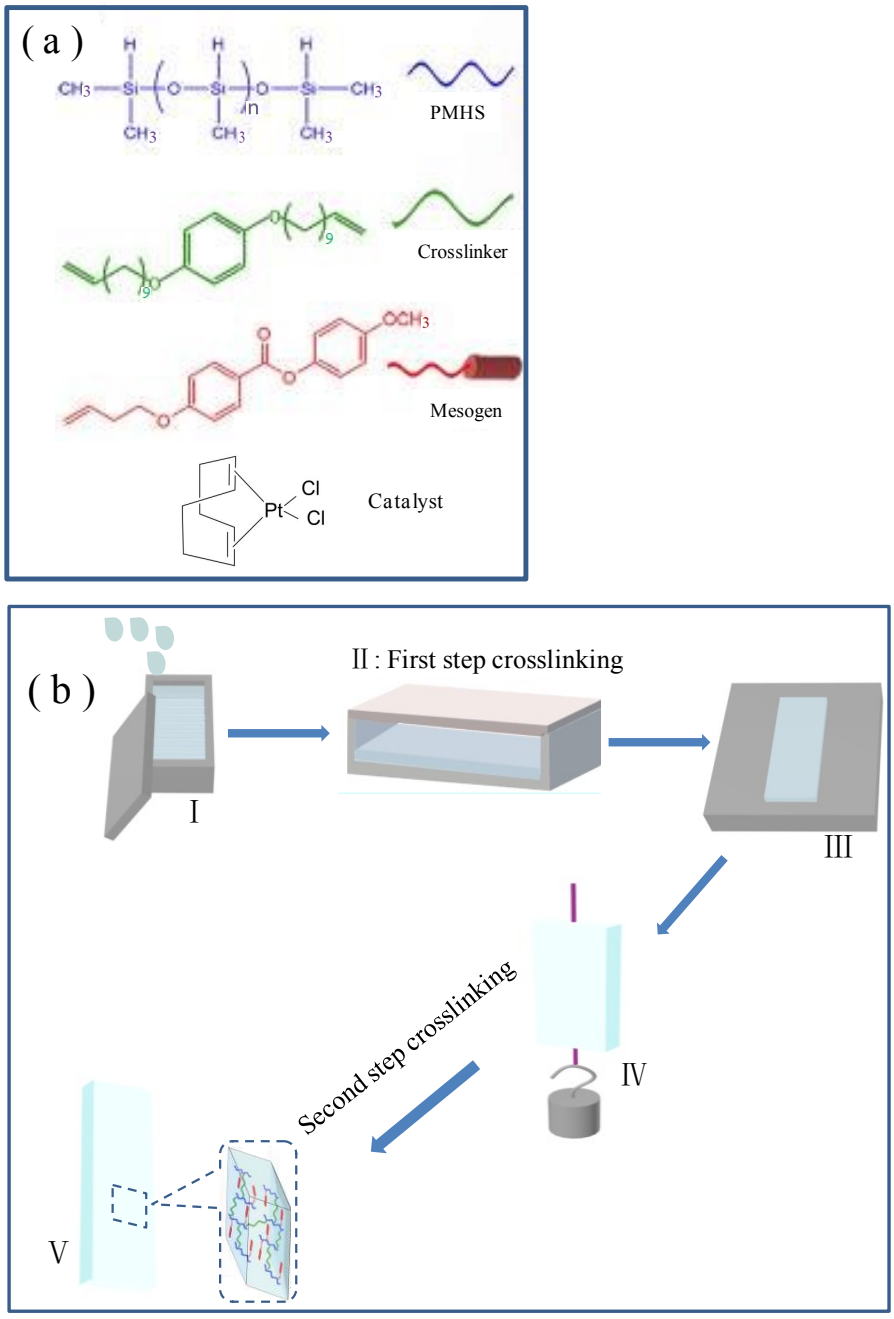

Scheme S1. Illustration for the molecular structures of precursor reactants (a) and the preparation of polysiloxane side-chain LCE (b). (b-Ⅰ) Pouring the precursor reactant mixture, which was composed

of PMHS, MBB, 11UB and $Pt(COD)Cl_2$ catalyst solution dissolved in toluene, into a Teflon mold. (b-Ⅱ) The mold was put in an oven in 65 °C for 40 min to achieve the first step crosslinking and generate a partially crosslinked swollen gel. (b-Ⅲ) The generated partially crosslinked swollen gel was transferred out of the mold and dried in air for 40 minutes to let the contained toluene fully evaporated. (b-Ⅳ) The generated de-swollen partially crosslinked elastomer was slowly uniaxially stretched under a load for 12 hours to attain a stable length and form the nematic phase in matrix network which was confirmed by the POM observation shown in Figure S2. (b-Ⅴ) The elastomer with the load was heated at 70°C overnight to complete the second step crosslinking and obtained the monodomain nematic LCE with axial alignment of mesogens. The dimension of the prepared LCE material was 40 mm × 10 mm × 0.5 mm.

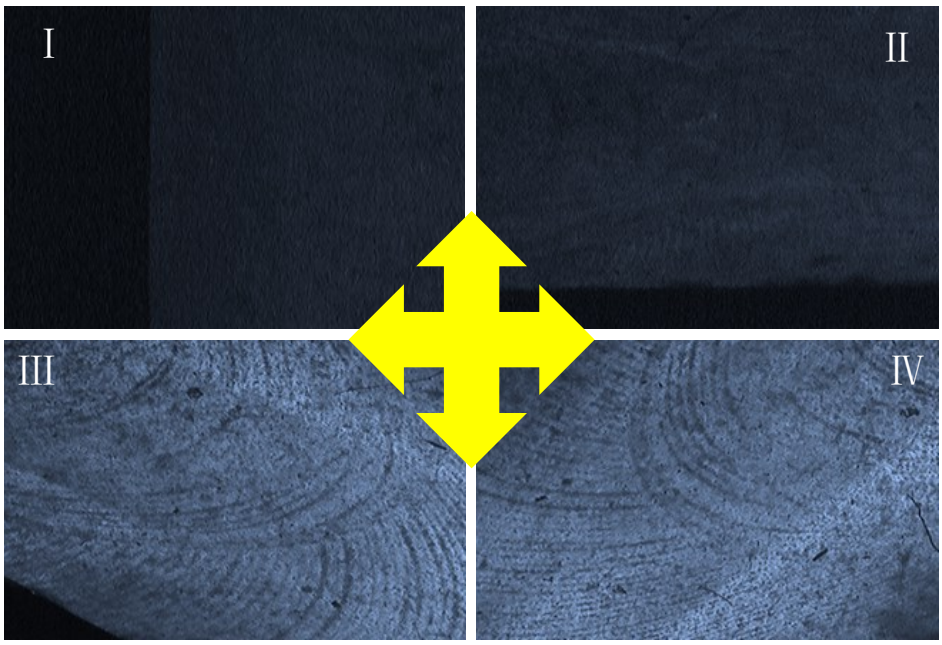

Figure S1. POM images of the partially crosslinked elastomer after being stretched and before the second step crosslinking, inserted crossarrows illustrate the polarization directions of the two polarizers: The stretch direction of the partially crosslinked elastomer sample is parallel to the vertical polarization direction (Ⅰ), parallel to the horizontal polarization direction (Ⅱ), tilted at an angle of -45º to either polarization direction (Ⅲ), and tilted at an angle of 45º to either polarization direction (Ⅳ).

Figure S1 shows the POM images of a partially crosslinked elastomer sample which was uniaxially stretched under a load for 12 hours before the second step crosslinking. The sample showed the minimum transmittance when its stretch direction was parallel or perpendicular to one of the polarizers, while highest transmittance appeared when its

stretch direction tilted at an angle of ±45° to the polarizers. The POM observation confirmed that the nematic structure was already formed in the partially crosslinked elastomer after being stretched, and that the mesogens were axially aligned along the stretch direction.

S-Ⅱ: The discussion of ATR-FTIR spectrum.

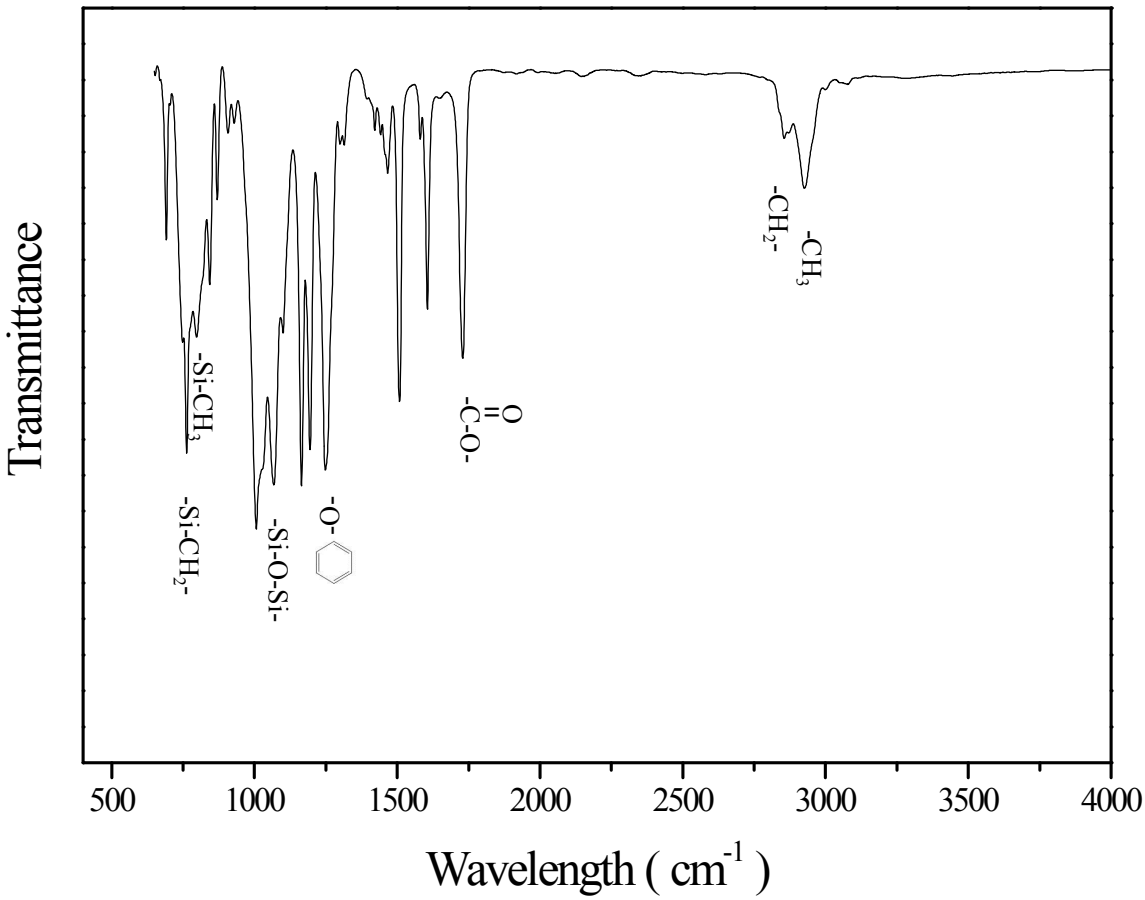

Figure S2. ATR-FTIR spectrum of the prepared polysiloxane side-chain LCE.

Figure S2 shows the measured ATR-FTIR spectrum of the prepared polysiloxane side-chain LCE. The sample exhibited the characteristic peaks of molecular functional groups contained in MBB, 11UB and PMHS:[S1] the peak at about 2942 cm^{-1} was attributed to the vibration of methyl groups ($-CH_3$), the peak at about 2865 cm^{-1} was attributed to the vibration of aliphatic methylene ($-CH_2-$), the peak at about 1730 cm^{-1} was attributed to the

ester carbonyl group (-C=O) vibration, the peak at about 1250 cm^{-1} was attributed to the vibration of alkyl-aryl ether (aryl-O-), the peak at around 1070 cm^{-1} was attributed to the vibration of silicon-oxygen bonds (Si-O-Si), the peak at about 795 cm^{-1} was attributed to the vibration of silicon methyl bonds ($Si-CH_3$). But there were no detected characteristic peaks of ethylenic bond (C=C) at about 1620-1680 cm^{-1}, alkenyl hydrogen bonds ($=CH_2$) at about 3000-3100 $cm^{-1}$and silicon hydrogen bond (Si-H) at about 2160 cm^{-1}, instead the vibration peak of silicon methylene ($Si-CH_2-$) at about 760 cm^{-1} was obviously exhibited. The reason should be that the Si–H bonds in the PMHS reacted with the terminal vinyl groups of MBB molecules and 11UB molecules and hence generated the silicon methylene ($Si-CH_2-$) bonds. Therefore the ATR-FTIR spectrum confirmed that the LCE network was synthesized through hydrosilation crosslinking reaction as demonstrated in Scheme 1.

S-Ⅲ: The volumetric heat generation and mechanical power.

Fig.4 (a) shows the axial strains of LCE versus microwave irradiation intensity at different irradiation time, and Fig.4 (b) shows the temperatures of LCE in response to microwave stimulus versus irradiation intensity at different irradiation time. It indicated from Fig. 4 that the axial contraction strain reached the maximum contraction strain, which was about 32.5%, after 55 seconds of irradiation with the intensity of 6 mW/cm^2, and the temperature of the LCE material increased from 20℃ to 77.75℃. The loading stress undertaken by the LCE material during the contraction process was 70 kPa. The received irradiation energy is "$E=I\times S\times \Delta t$". The volumetric heat increasing is "$\Delta H=\rho\times V\times c\times \Delta T$". The powered work of contraction is "$W=p\times \Delta s\times \Delta L$". Here, I is the irradiation intensity, S is the front surface area of the LCE material, Δt is the time interval, ρ is the density, V is the material volume, c is the thermal capacity, ΔT is the temperature increase, p is the loading stress, Δs is the cross-sectional area of the material, ΔL is the length change of the contraction process. Based on the material parameters and parametric variations. The

calculated irradiation energy, volumetric heat and powered work was 1.32J, 2.08×10^{-2}J and 4.62×10^{-3}J respective. The calculated efficiency from irradiation energy to volumetric heat, which should be the ratio of the volumetric heat to the irradiation energy, was about 1.58%. The calculated efficiency from irradiation energy to powered work, which should be the ratio of the powered work to the irradiation energy, was about 0.35%. The irradiation energy did not totally converted into the volumetric heat and the powered work, the reason should be that major part of the irradiation energy penetrated through the material, and part generated heat dissipated into the environment.

S-Ⅳ: The microwave detector system.

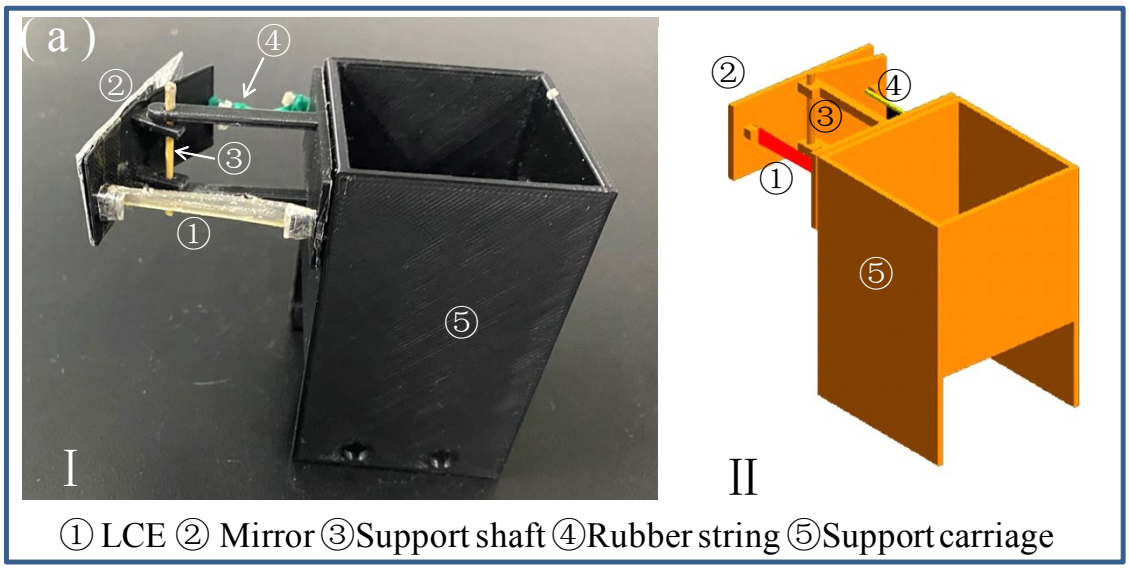

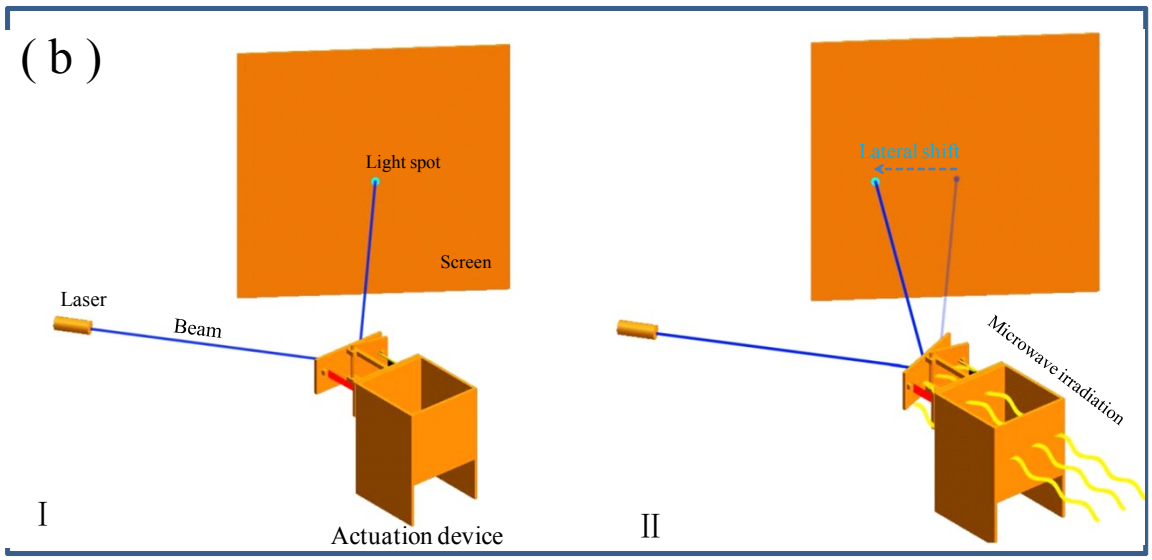

Figure S3. (a) The photo image (Ⅰ) and the schematic setup (Ⅱ) of the actuation device for the microwave detector system. (b-Ⅰ) The schematic setup of the microwave detector system. (b-Ⅱ) The

schematic illustration for the implementation process of the microwave detector system.

Figure S3a-Ⅰ and Figure S3a-Ⅱ respectively show the photo image and the schematic setup of the actuation device for the microwave detector system, and every component of the actuation device is signed. A LCE material with 40mm of length was acted as the actuator material. The setup of the microwave detector system is illustrated in Figure S3b. The mirror installed on the actuation device was illuminated by a laser beam, and the reflected beam was received by a screen, forming a light spot on the screen, as shown in Figure S3b-Ⅰ. Figure S3b-Ⅱ illustrates the state of the microwave detector system when the microwave source was turned on. The microwave irradiated from the back wall of the support carriage of actuation device with the incidence direction paralleling to the axial direction of the LCE material. Due to its strong penetrability, the microwave penetrated the back wall and front wall of the support carriage, then penetrated the LCE from bottom to top and actuated the LCE material. The LCE contracted, tilting the mirror, and therefore, changing the direction of the reflected beam. As a result, the light spot on the screen laterally shifted. After the microwave source was turned off, the LCE material started to recover to its initial length. During the recovering process, by the aid of elasticity of the rubber string fixed on the other end of the mirror, the tilt angle of mirror returned to zero of initial state. As a result, the light spot on the screen returned back to its initial position.

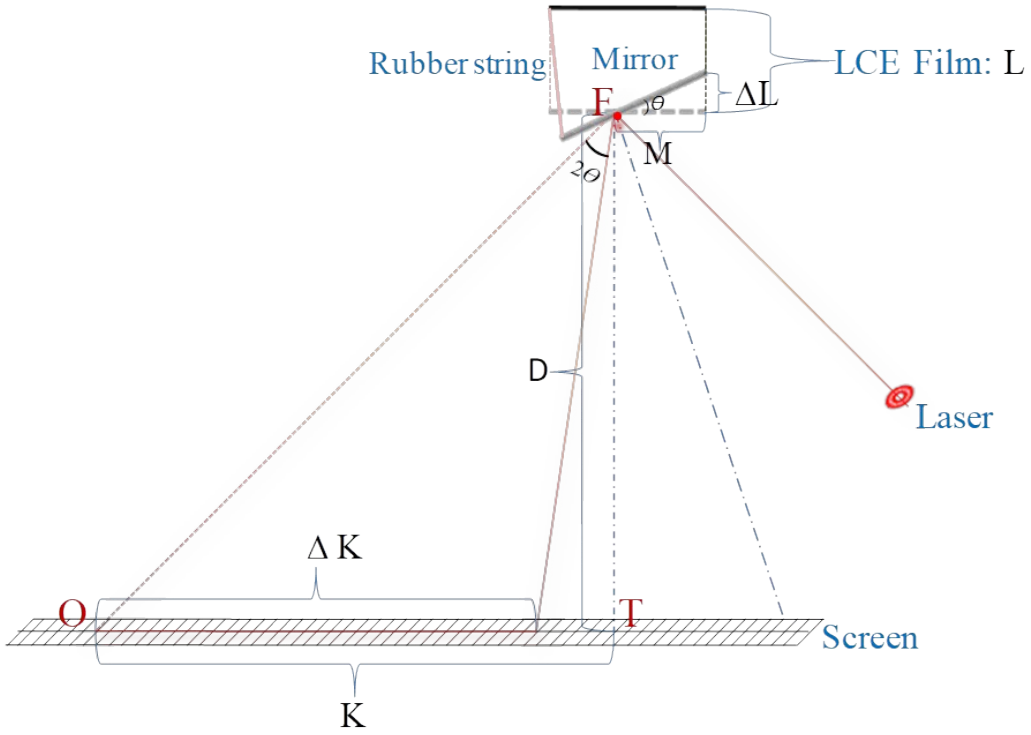

Scheme S2. The model for the lateral displacement of light spot on the screen induced by the contraction of the LCE upon microwave irradiation.

To analyze the light spot displacement on the screen induced by the microwave irradiation, a model is illustrated in Scheme S2. Where, "L" is the original length of LCE material; "D" is the distance between mirror and screen; "M" is the length between the beam incidence point on the mirror "F" and the right end of the mirror; The straight line "FT" from point "F" is vertical to the screen, and point "T" is the intersection point between straight line "FT" and the screen. "K" is the distance between the initial light spot "O" on the screen and point "T"; "ΔL" is the contraction length of LCE driven by the microwave irradiation; "θ" is the tilt angle of the mirror caused by the contraction of LCE; "ΔK" is the lateral displacement of the light spot on the screen. Through the mathematical derivation, it is derived as follows:

$$2\Theta = arctan(K/D) - arctan\frac{K - \Delta K}{D} \quad (1)$$

$$\Delta L = M tan\theta \qquad (2)$$

Here, K=218mm; D=200mm; M=38mm; L=40mm. If the value of ΔL is determined, the value of ΔK can be calculated by combining and solving the equation (1) and (2).

When a small contraction strain, such as 1%, of LCE is happened, then the ΔL= L×1%=0.4mm, the calculated ΔK is 10.42mm. The magnification is calculated as: n=ΔK /ΔL=26.05.

When the maximum contraction strain, about 33%, of LCE is happened, then the ΔL= L×33%=13.2mm, the calculated ΔK is 188.35mm. The magnification is calculated as: n=ΔK /ΔL=14.27.

It is revealed from above analysis that the shift displacement of the light spot on the screen can be several tens of times than the contraction length of LCE material, and a very small contraction strain of LCE material will bring an obvious shift displacement of the light spot on the screen. Thus the microwave detector system had a well sensitivity.

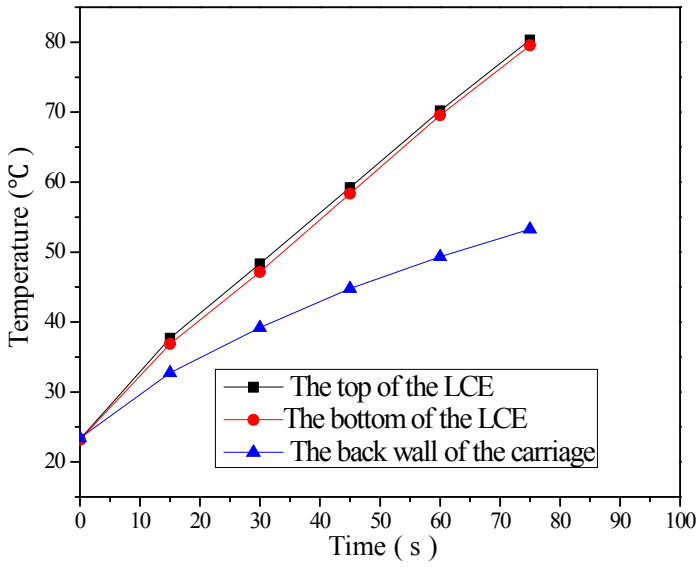

Figure S4. The temperatures at the top of the LCE, the bottom of the LCE and the back wall of the carriage at different time of microwave irradiation. The microwave irradiation intensity at the back wall place of the support carriage was 7.0 mW/cm^2.

The temperatures at different locations of the LCE actuator in the microwave detector system were tested at different time during the microwave irradiation process. As shown in Figure S4, it indicated that the temperatures at the LCE actuator and the back wall of the carriage increased as the irradiation time prolonged. There was no obvious difference between the temperatures at the top of the LCE and the bottom of the LCE. This should be attributed to the high penetrability of microwave irradiation and the shorter length of the LCE actuator, which led to nearly uniform volumetric heating in the whole LCE material. Figure S4 indicates that the temperatures at the back wall of the carriage were lower than those at the LCE actuator at different time during the irradiation, though the back wall of the carriage was nearer to the microwave source relative to the LCE actuator. The reason should lie in the different properties of the two materials.

Reference

[S1] P. J. Larkin, *Infrared and Raman spectroscopy: Principles and spectral interpretation*. Elsevier, USA **2011**.